New generalized blended trigonometric Bézier curves with one shape parameter

Harmanjit Kaur[a], Meenu Rani Goyal[a,*]

[a]*School of Mathematics, Thapar Institute of Engineering and Technology, Patiala-147004, India*

Abstract. This paper introduces a new basis for generalized blended trigonometric (GBT) Bézier curves along with one shape parameter. The recursive technique is adopted to formulate the basis for higher order GBT-Bézier curves. The curves are better approximated using the proposed basis than the traditional Bernstein basis. New basis functions and curves satisfy all the properties followed by classical Bézier curves. The shape of these curves can be adjusted by changing the values of the parameter, keeping the control polygon unchanged. This adds to the flexibility of new GBT-Bézier curves. Appropriate conditions for parametric (C^0, C^1, C^2 and C^3) and geometric (G^0, G^1, G^2 and G^3) continuities to compose two or more GBT-Bézier curves have been worked upon. Applications of the proposed GBT-Bézier curves are discussed with different formations.

1. Introduction

Bézier curves have become indispensable instruments to understand the work involved in various applications ranging from CAGD to generic object shape descriptors. There are numerous applications of Bézier curves in time domains like animation, interface design, describing font characters, image compression, highway modeling, robotics, and many other fields [16]. Bézier curves are parametric curves that use Bernstein polynomials as basis functions [23]. These curves are popularized since their mathematical descriptions are compact, easy to compute, and quite stable. Bézier from Renault had a significant impact in this context. He played a key role in the creation of Bézier curves, a potent tool for creating free-form curves and surfaces. This motivated several researchers to work upon the Bézier variant of different p.l.o. and applications of generalizations corresponding to the p.l.o. in various fields [22]. Acar and Agrawal [1] introduced the Bézier-variant of Durrmeyer modification of the Bernstein operators based on a function τ, which is infinite times continuously differentiable and strictly increasing function on [0, 1]. Similar work has been done for Bernstein-Durrmeyer-type operators, summation-integral-type operators and Srivastava-Gupta-type operators in [2], [13] and [14] respectively. Despite these advantages, classical Bézier curves have some constraints as their control polygons fix the shape and position of the curves. So, shape adjustability is only possible by altering the control points in the case of traditional Bézier curves. In CAD/CAM technology areas, the flexibility of these curves is a subject of concern. Designing and changing

shapes is a tedious and time taking task in classical Bézier curves. These drawbacks are vanquished by using shape parameters in trigonometric Bézier curves as they prove to be a better choice for spiral or circular formations as compared to polynomial Bézier curves with shape parameters.

Over the last few years, a number of researchers have used diversified bases with varying ranges of shape parameters to define Bézier curves to overcome the limitations of classical Bézier curves. In [8], Han provided the references for initially available literature and constructed quadratic trigonometric polynomial curves parallel to quadratic B-spline curves. The study was held forth for cubic trigonometric curves in [9, 11]. Quintic trigonometric Bézier curves with two shape parameters were introduced by Misro et al. in [20]. In [27], Uzma et al. constructed trigonometric Bézier curves of degree 2 (QT-Bézier curves) with single shape parameter, which were used for representing ellipse. Authors concluded that QT-Bézier curves were helpful in approximating circular arcs. Their work was further extended to cubic trigonometric Bézier curves (CBT-Bézier curves) with one shape parameter. Different bases were defined for cubic trigonometric Bézier curves in [17, 25] and [7, 24] can be referred to for quartic trigonometric Bézier curves. A generalization of Bernstein basis functions was introduced along with n shape parameters by Han [10] to generate Quasi Bézier (Q-Bézier) curves, continuity conditions for which have been studied in [12]. In [4], Bashir et al. introduced two parameters for quasi-quintic trigonometric Bézier curves. Some engineering applications of the cubic trigonometric curves have been discussed in [26] along with C^1, C^2 parametric continuities and G^1, G^2 geometric continuities. Conditions for G^3 continuity are mentioned in [6] and [17]. Other papers that can be referred to study parametric and geometric continuities of trigonometric Bézier curves are [5, 21].

As the study of these curves gained pace, numerous researchers stepped up to introduce shape parameters varying over different intervals. Our work is motivated by Ammad et al. [3] and Maqsood et al. [18] in which the authors generalized the trigonometric Bézier curves and introduced two shape parameters. The recurrence technique having trigonometric functions was opted to generalize the results. In a subsequent paper, Maqsood et al. [19] improved this recursive formula by introducing algebraic and trigonometric functions for defining the mth order Generalized Blended Trigonometric Bézier curves with two shape parameters.

In this paper, we introduce the new GBT-Bernstein-like basis with one shape parameter for mth degree using the recursive technique formulated in [19]. The conditions for parametric continuity are stated to compose multiple Bézier curves which are helpful in designing complex structures. The curves formed using new basis have more flexibility and shape adaptability which lacked in classical Bézier curves.

The layout of the paper is as follows. Section 2 consists of definitions and properties associated with the new GBT-basis functions. Construction of corresponding new GBT-Bézier curves is dealt with in Section 3 along with the properties of the curves. In Section 4, we have introduced the conditions for composing two or more Bézier curves which require parametric continuity, and examples related to different parametric constraints are plotted for curves of degrees 3, 4, and 5. Geometric constraints of the proposed basis functions and examples corresponding to these curves are discussed in the same section. The final arguments are concluded in Section 5 of the paper.

2. Definition and properties of new generalized blended trigonometric Bézier curves

We introduce the new GBT-basis functions and further define the recursive technique in this section.

2.1. New GBT-basis functions

Definition 1: For an arbitrary shape parameter $\alpha \in [-2, 1)$ and $z \in [0, 1]$, the functions

$$\beta_{0,2}(\alpha, z) = \frac{1}{2}(1 - \sin\frac{\pi}{2}z)\left[(1 - \alpha\sin\frac{\pi}{2}z) + \cos\frac{\pi}{2}z\right]$$

$$\beta_{2,2}(\alpha, z) = \frac{1}{2}(1 - \cos\frac{\pi}{2}z)\left[(1 - \alpha\cos\frac{\pi}{2}z) + \sin\frac{\pi}{2}z\right]$$

$\beta_{1,2}(\alpha, z) = 1 - \beta_{0,2}(\alpha, z) - \beta_{2,2}(\alpha, z)$ are called the second degree new GBT-basis functions.

In contemplation of defining new basis $\beta_{i,m}(\alpha, z)$ $(i = 0, 1, ..., m)$ for degree $m \geq 3$, recursive technique has been used as below:

$\beta_{i,m}(\alpha, z) = (1 - z)\beta_{i,m-1}(\alpha, z) + z\beta_{i-1,m-1}(\alpha, z)$ where $\beta_{i,m}(\alpha, z) = 0$ when $i = -1$ or $i > m$.

Figure 1 provides the comparison between the basis functions of new GBT and classical Bézier curves. It is evident that the new GBT basis functions provide more flexibility for the varying values of shape parameter $\alpha \in [-2, 1)$. Blue color indicates the classical Bernstein basis functions whereas red and black color is used to indicate the new GBT-basis functions for $\alpha = 0.99$ and $\alpha = -2$ respectively.
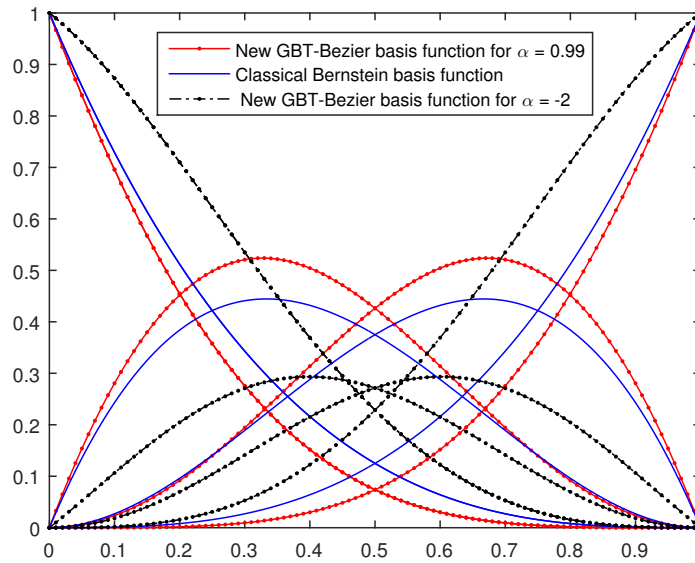
Figure 1: Comparison between the basis functions of new GBT and classical Bernstein Bézier curves

2.2. Properties of new basis functions

The new basis functions $\beta_{i,m}(\alpha, z)$ have the following properties:

1. **Partition of unity:** $\sum_{i=0}^{m} \beta_{i,m}(\alpha, z) = 1$, which can be proved by inductive hypothesis.

   For "m" = 2, we have: $\sum_{i=0}^{2} \beta_{i,2}(\alpha, z) = 1$ (Obvious by Definition 1).

   Let us assume this is true for $m = k$ i.e. $\sum_{i=0}^{k} \beta_{i,k}(\alpha, z) = 1$.

   Therefore, if we choose $m = k + 1$, then according to the recursive formula for defining a new GBT-Bézier basis of degree m, we can write:

$$\sum_{i=0}^{k+1} \beta_{i,k+1}(\alpha,z) = \sum_{i=0}^{k+1} \left[(1-z)\beta_{i,k}(\alpha,z) + z\beta_{i-1,k}(\alpha,z) \right]$$

$$= \sum_{i=0}^{k+1} (1-z)\beta_{i,k}(\alpha,z) + \sum_{i=0}^{k+1} z\beta_{i-1,k}(\alpha,z)$$

$$= (1-z)\left[\sum_{i=0}^{k} \beta_{i,k}(\alpha,z) + \beta_{k+1,k}(\alpha,z) \right] + z\left[\sum_{i=0}^{k} \beta_{i,k}(\alpha,z) + \beta_{-1,k}(\alpha,z) \right]$$

$$= (1-z)(1+0) + z(1+0) = 1.$$

2. **Non-negativity:** For shape parameter $\alpha \in [-2,1)$ and $z \in [0,1]$, we have $\beta_{i,m}(\alpha,z) \geq 0$ for $i = 0,1,...,m$. Since $(1 - \sin\frac{\pi}{2}z) \geq 0$, $(1 - \alpha\sin\frac{\pi}{2}z) \geq 0 \ \forall \ \alpha \in [-2,1)$ along with $\cos\frac{\pi}{2}z \geq 0$, we get that $\beta_{0,2}(\alpha,z) \geq 0$. On similar grounds it can be proved that $\beta_{1,2}(\alpha,z)$ and $\beta_{2,2}(\alpha,z)$ are non-negative. For higher degree bases we have the recursive technique which involves the combination of $(1-z)$ and z. Since $z \in [0,1]$ and $\beta_{i,m-1}(\alpha,z)$ and $\beta_{i-1,m-1}(\alpha,z) \geq 0$, therefore $\beta_{i,m}(\alpha,z)$ is non negative $\forall z \in [0,1]$. It is verified graphically as in Figure 2. It also represents the effect of varying the shape parameter on the new GBT-basis functions.
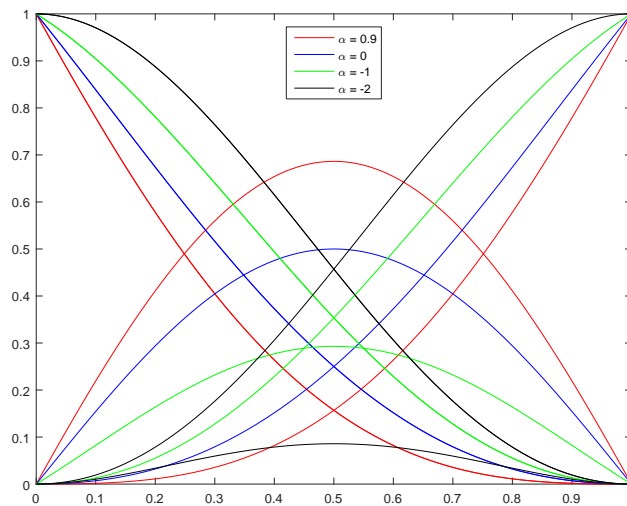
Figure 2: Non-negativity property of new GBT-basis functions

3. **Terminal property:** The basis functions at the end points are given by:

$$\beta_{i,m}(\alpha,0) = \begin{cases} 1, & i = 0 \\ 0, & i = 1,2,...,m. \end{cases} \tag{1}$$

$$\beta_{i,m}(\alpha,1) = \begin{cases} 1, & i = m \\ 0, & i = 0,2,...,m-1. \end{cases} \tag{2}$$

4. **Symmetry:** The basis functions follow a symmetry throughout, *i.e.* if $p_0, p_1, ..., p_m$ are $m + 1$ control points then, $\beta_{i,m}(\alpha, z, p_0, p_1, ..., p_m) = \beta_{m-i,m}(\alpha, 1 - z, p_m, p_{m-1}, ..., p_1, p_0)$, for $i = 0, 1, ..., m$. For $m = 2$, we have:

$$\beta_{i,2}(\alpha, z) = \beta_{2-i,2}(\alpha, 1 - z).$$

Let us assume this holds true for $m = k$ i.e.

$$\beta_{i,k}(\alpha, z) = \beta_{k-i,k}(\alpha, 1 - z).$$

So, as we choose $m = k + 1$ and apply the recursive technique, we get

$$\begin{aligned}
\beta_{i,k+1}(\alpha, 1 - z) &= z \, \beta_{i,k}(\alpha, 1 - z) + (1 - z) \, \beta_{i-1,k}(\alpha, 1 - z) \\
&= z \, \beta_{k-i,k}(\alpha, z) + (1 - z) \, \beta_{k+1-i,k}(\alpha, z) \\
&= (1 - z) \, \beta_{k+1-i,k}(\alpha, z) + z \, \beta_{k-i,k}(\alpha, z) \\
&= \beta_{k+1-i,k+1}(\alpha, z).
\end{aligned}$$

3. Constructing new GBT-Bézier curves

For given $m + 1$ control points p_i ($i = 0, 1, ..., m$) in $\mathbb{R}^2$, the new GBT-Bézier curve of degree m with shape parameter α is defined as following:

$$r(\alpha, z) = \sum_{i=0}^{m} \beta_{i,m}(\alpha, z) * p_i, \quad z \in [0, 1], \alpha \in [-2, 1).$$

3.1. Properties of new GBT-Bézier curves

The new GBT-Bézier curves satisfy the following properties:

1. **Endpoint interpolation:** The new proposed GBT-Bézier curve passes through the initial and final control points i.e.

$$r(\alpha, 0) = p_0,$$
$$r(\alpha, 1) = p_m.$$

Here p_0 & p_m are initial and final points respectively.

2. **Convex hull property:** Since the basis functions are non-negative and follow the property of partition of unity, the curve formed with the help of control points assigned will always lie within the convex hull of the control polygon.

3. **Geometric invariance:** The shape of the GBT-Bézier curve doesn't depend upon the coordinates chosen, i.e. the following equations are satisfied:

$$r(z; \alpha; p_0 + v, p_1 + v, ..., p_m + v) = r(z; \alpha; p_0, p_1, ..., p_m) + v$$

where v is arbitrary vector in $\mathbb{R}^2$.

4. **Derivatives at endpoints:** The value of derivatives at initial and final points is given by:

$$\beta'_{i,m}(\alpha, 0) = \begin{cases} -\left[\frac{\pi}{4}(\alpha + 2) + m_2\right], & i = 0 \\[2mm] \left[\frac{\pi}{4}(\alpha + 2) + m_2\right], & i = 1 \\[2mm] 0, & \textit{otherwise.} \end{cases} \tag{3}$$

$$\beta'_{i,m}(\alpha, 1) = \begin{cases} -\left[\frac{\pi}{4}(\alpha + 2) + m_2\right], & i = m - 1 \\ \\ \left[\frac{\pi}{4}(\alpha + 2) + m_2\right], & i = m \\ \\ 0, & otherwise. \end{cases} \tag{4}$$

$$\beta''_{i,m}(\alpha, 0) = \begin{cases} \frac{\pi^2}{8}(2\alpha - 1) + \frac{\pi}{2}(\alpha + 2)m_2 + m_2 m_3, & i = 0 \\ \\ -\frac{\pi^2}{8}\alpha - \pi(\alpha + 2)m_2 - 2m_2 m_3, & i = 1 \\ \\ -\frac{\pi^2}{8}(\alpha - 1) + \frac{\pi}{2}(\alpha + 2)m_2 + m_2 m_3, & i = 2 \\ \\ 0, & otherwise. \end{cases} \tag{5}$$

$$\beta''_{i,m}(\alpha, 1) = \begin{cases} -\frac{\pi^2}{8}(\alpha - 1) + \frac{\pi}{2}(\alpha + 2)m_2 + m_2 m_3, & i = m - 2 \\ \\ -\frac{\pi^2}{8}\alpha - \pi(\alpha + 2)m_2 - 2m_2 m_3, & i = m - 1 \\ \\ \frac{\pi^2}{8}(2\alpha - 1) + \frac{\pi}{2}(\alpha + 2)m_2 + m_2 m_3, & i = m \\ \\ 0, & otherwise. \end{cases} \tag{6}$$

$$\beta'''_{i,m}(\alpha, 0) = \begin{cases} \frac{\pi^3}{16}(\alpha + 5) - \frac{3\pi^2}{8}(2\alpha - 1)m_2 - \frac{3\pi}{4}(\alpha + 2)m_2 m_3 - m_2 m_3 m_4, & i = 0 \\ \\ -\frac{\pi^3}{16}(\alpha + 8) + \frac{3\pi^2}{8}(3\alpha - 1)m_2 + \frac{3\pi}{4}(\alpha + 2)3m_2 m_3 + 3m_2 m_3 m_4, & i = 1 \\ \\ \frac{3\pi^3}{16} - \frac{3\pi^2}{8}m_2 - \frac{3\pi}{4}(\alpha + 2)3m_2 m_3 - 3m_2 m_3 m_4, & i = 2 \\ \\ \frac{-3\pi^2}{8}(\alpha - 1)m_2 + \frac{3\pi}{4}(\alpha + 2)m_2 m_3 + m_2 m_3 m_4, & i = 3 \\ \\ 0, & otherwise. \end{cases} \tag{7}$$

$$\beta'''_{i,m}(\alpha,1) = \begin{cases} \frac{3\pi^2}{8}(\alpha-1)m_2 - \frac{3\pi}{4}(\alpha+2)m_2m_3 - m_2m_3m_4, \ i = m-3 \\[2ex] \frac{-3\pi^3}{16} + \frac{3\pi^2}{8}m_2 + \frac{3\pi}{4}(\alpha+2)3m_2m_3 + 3m_2m_3m_4, \ i = m-2 \\[2ex] \frac{\pi^3}{16}(\alpha+8) - \frac{3\pi^2}{8}(3\alpha-1)m_2 - \frac{3\pi}{4}(\alpha+2)3m_2m_3 - 3m_2m_3m_4, \ i = m-1 \\[2ex] -\frac{\pi^3}{16}(\alpha+5) + \frac{3\pi^2}{8}(2\alpha-1)m_2 + \frac{3\pi}{4}(\alpha+2)m_2m_3 + m_2m_3m_4, \ i = m \\[2ex] 0, \ otherwise. \end{cases} \tag{8}$$

Here, $m_2 = m-2$, $m_3 = m-3$, $m_4 = m-4$ and m is the degree of the new GBT curve.

4. Composition of new GBT-Bézier curves

During the formation of complex figures, we need to join multiple curves in order to obtain the desired structure. Thus for the composition of new GBT-Bézier curves, conditions for parametric and geometric continuities need to be worked upon. Section 4 provides the constraints for the same. This section is further divided into two subsections. Subsection 4.1 provides the conditions for the composition of new GBT-Bézier curves that follow parametric continuities. Subsection 4.2 helps us in understanding the constraints required to compose new GBT-Bézier curves that follow geometric continuities. The applicability of the parametric and geometric continuity constraints is demonstrated in 4.1.1 and 4.2.1 respectively. To begin with, let us consider new GBT-Bézier curves as defined by equation (9)

$$\begin{cases} r(\alpha,z) = \sum_{i=0}^{m} \beta_{i,m}(\alpha,z) * p_i, \ z \in [0,1], \alpha \in [-2,1), \\[2ex] s(\alpha,z) = \sum_{i=0}^{m} \beta_{i,m}(\alpha,z) * q_i, \ z \in [0,1], \alpha \in [-2,1), \end{cases} \tag{9}$$

where p_i and q_i are control points for the new GBT-Bézier curves $r(\alpha,z)$ & $s(\alpha,z)$ respectively and $\beta_{i,m}(\alpha,z)$ represent the new basis functions.
Also, we have

$$r(\alpha,0) = p_0, \ r(\alpha,1) = p_m$$

and

$$s(\alpha,0) = q_0, \ s(\alpha,1) = q_m$$

where p_0 & q_0 are initial control points of the first curve $r(\alpha,z)$ and second curve $s(\alpha,z)$ respectively and p_m & q_m are final control points of the first curve $r(\alpha,z)$ and second curve $s(\alpha,z)$ respectively.

4.1. Parametric continuity constraints of new GBT-Bézier curves

Computer-Aided Geometric Design (CAGD) is used in aerospace, automotive, ship building, pharmaceutical design, animation, etc. During virtual prototyping, multiple curves are used to obtain the final design. To ensure the smoothness of the curves involved in the process of expected outcomes, parametric continuity is imperative. In this section, we have worked on the required parametric continuity constraints.
Theorem 4.1: The necessary and adequate constraints for parametric continuity between two GBT-Bézier curves as defined in equation (9) are given by:

1. Conditions for C^0 continuity: The value of the first curve at "$z = 1$" must be equal to the value of second curve at "$z = 0$" *i.e.* $r(\alpha, 1) = s(\alpha, 0)$. This means that the beginning of the second curve marks the ending of the first curve as shown in figure 3 *i.e.* $p_4 = q_0$. Since $r(\alpha, 1) = p_m$ and $s(\alpha, 0) = q_0$, this leads to the constraint for C^0 continuity as:

$$q_0 = p_m. \tag{10}$$
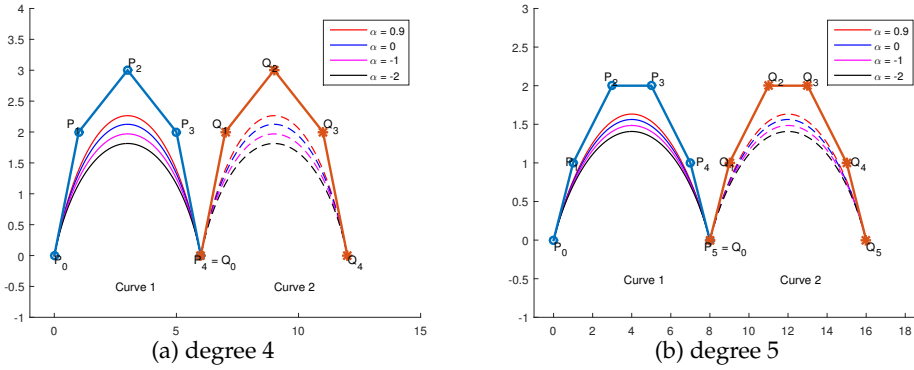
Figure 3: Composition of C^0 continuous graphs

2. Conditions for C^1 continuity: Along with the constraints of C^0 continuity, the curve has to follow additional condition that the first derivative of first curve at "$z = 1$" must be equal to the first derivative of the second curve at "$z = 0$" *i.e.* $r(\alpha, 1) = s(\alpha, 0)$ and $r'(\alpha, 1) = s'(\alpha, 0)$. Thus, we get the conditions for C^1 continuity as:

$$\begin{cases} q_0 = p_m \\ q_1 = 2p_m - p_{m-1}. \end{cases} \tag{11}$$

Hence, C^1 continuity can be visualized through Figure 4, exhibiting common tangents to both the curves.
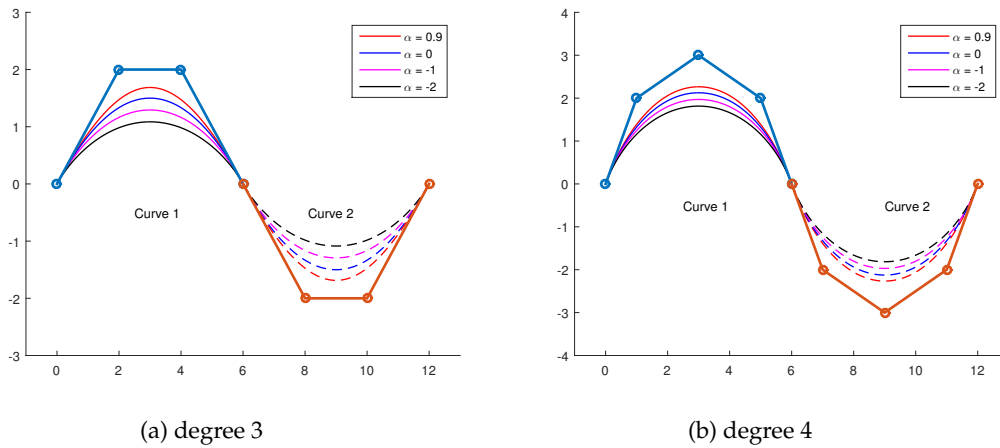
Figure 4: Composition of C^1 continuous graphs

3. Conditions for C^2 continuity: C^2 continuity provides a smooth transition between the curves by flattening them at the point of confluence which can be seen in Figure 5. These constraints are obtained by

using $r(\alpha, 1) = s(\alpha, 0)$, $r'(\alpha, 1) = s'(\alpha, 0)$ and $r''(\alpha, 1) = s''(\alpha, 0)$ leading to the following conditions:

$$
\begin{cases}
q_0 = p_m \\
\\
q_1 = 2p_m - p_{m-1} \\
\\
q_2 = p_{m-2} - \dfrac{2\beta''_{1,m}(\alpha,0)}{\beta''_{2,m}(\alpha,0)}(p_m - p_{m-1})
\end{cases}
\tag{12}
$$

(a) degree 4   (b) degree 5
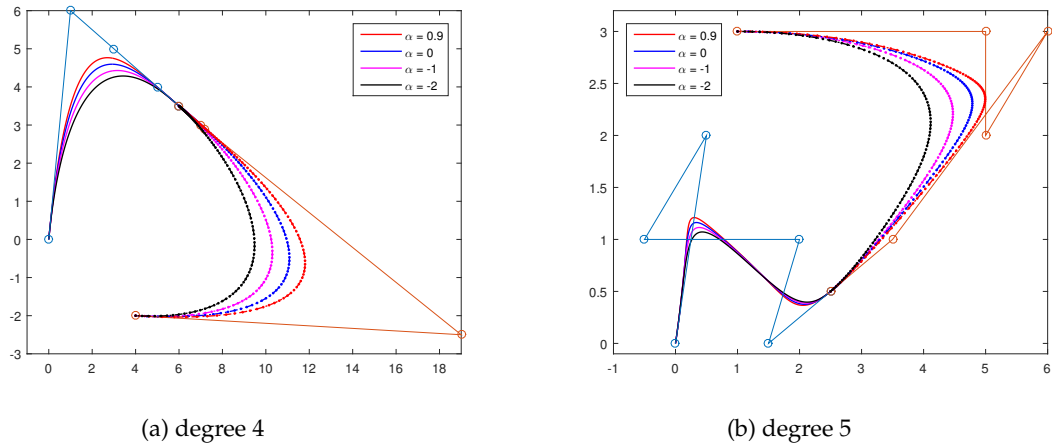
Figure 5: Composition of C^2 continuous curves

4. Conditions for C^3 continuity: Considering $r(\alpha, 1) = s(\alpha, 0)$, $r'(\alpha, 1) = s'(\alpha, 0)$, $r''(\alpha, 1) = s''(\alpha, 0)$ and $r'''(\alpha, 1) = s'''(\alpha, 0)$, we get the constraints for C^3 continuity of the curves:

$$
\begin{cases}
q_0 = p_m \\
\\
q_1 = 2p_m - p_{m-1} \\
\\
q_2 = p_{m-2} - \dfrac{2\beta''_{1,m}(\alpha,0)}{\beta''_{2,m}(\alpha,0)}\cdot(p_m - p_{m-1}) \\
\\
q_3 = -p_{m-3} - \left[2p_{m-2} - \dfrac{2\beta''_{1,m}(\alpha,0)}{\beta''_{2,m}(\alpha,0)}(p_m - p_{m-1})\right]\dfrac{\beta'''_{2,m}(\alpha,0)}{\beta'''_{3,m}(\alpha,0)} - 2p_m\dfrac{\beta'''_{1,m}(\alpha,0)+\beta'''_{0,m}(\alpha,0)}{\beta'''_{3,m}(\alpha,0)}.
\end{cases}
\tag{13}
$$

Figure 6 shows the composition of two new GBT-Bézier curves of degree six. The first curve (represented by solid lines) can be formed freely. The continuity constraints impose the conditions over control points of the second curve under consideration (represented by dotted lines). Once the first curve is drawn, we apply the C^3 continuity constraints given by equation (13) to extract the first four points of the second curve. The remaining control points can be chosen independently. The type of smoothness depends upon the applications of the curve. C^3 continuity comes into play when smoother curves are demanded.

With the introduction of shape parameter, the new GBT-Bézier curves procure versatility in their shapes. This property proves to be influential when it comes to the designing of complicated curves. The graphs related to parametric continuity of the curves in the previous subsection are formed using new basis functions with shape parameter $\alpha \in [-2, 1)$. In these figures (Figure: 3 - 6), the shifting of α is in black,
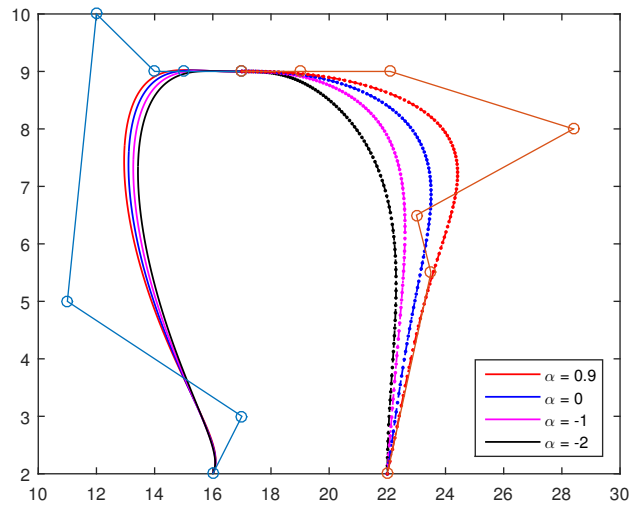
Figure 6: Composition of C^3 continuous curves of degree 6

magenta, blue and red lines corresponding to its value at -2, -1, 0 and 0.9 respectively. The solid lines indicate the variation of α over curve 1 and dotted lines are used to signify the alteration of α over curve 2. As we augment the shape parameter, the curve approaches the control polygon, giving a better approximation. Whereas, the classical Bézier curve generated a unique curve correlated to the given set of control points. Given that case to incorporate the desired changes, the control points of the classical Bézier curves had to be altered. On the contrary, the inclusion of the shape parameter in the basis functions saves us from this task. Moreover, it can be visualized graphically that every curve corresponding to various values of α satisfies the convex hull property and is non-negative.

4.1.1. Applications based on parametric continuity

This section deals with a variety of formations like flower, leaf, sparrow, heart-shaped, S-shaped, and spiral patterns created using new GBT-Bézier curves as an application to parametric continuities. The parameter $\alpha \in [-2, 1)$ varies according to the specification needed in the curve designing.

In Figure 7 and 8, the color red, green, blue, magenta and black is used to represent the values of α as 0.9, 0.5, 0, -1, -2 respectively. These figures demonstrate the variation in shapes, keeping control points fixed and therefore enhancing the flexibility during curve modeling.
Figure 7 (a)-(c) fore-shows a flower formation for curves of degrees three, four and five respectively. Condition derived in equation (10) for C^0 continuity has been imposed on these curves. Red, green and blue lines show the impact of changing parameter on the curve for positive values of α though red and black lines indicate the impact for negative values of α. It is evident from the figure that curve is closest to the control polygon for $\alpha = 0.9$. These figures can be further beautified by adding leaves and stalks of the flowers.
Figure 8 exhibits C^1 continuous curves using equation (11) where sub figures display (a) S-shaped, (b) spiral-shaped and (c) heart-shaped formations. Figure 8 also exemplifies the formation of conterminous curves requiring layered arcs. It represents curves of degree three in (a)-(b) and degree five in (c).
Application of C^2 continuity is designed in Figure 9. Additional conditions of C^2 continuity give constraints for first three points of the second curve involved and remaining points can be chosen freely. In Figure 9 (a), first curve (drawn using solid black arc) is formed by choosing $\alpha = -2$. We have used five control points for each arc, to obtain curves of degree four. The next five control points for the curve in red color
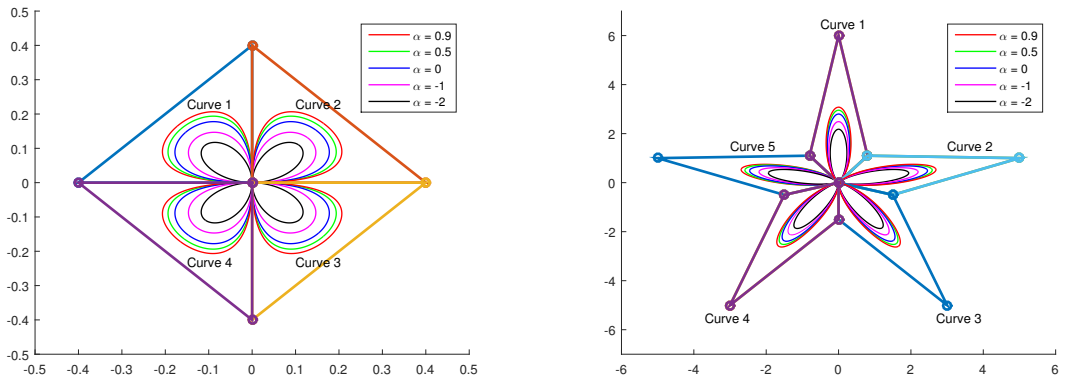
(a) Degree 3

(b) Degree 4
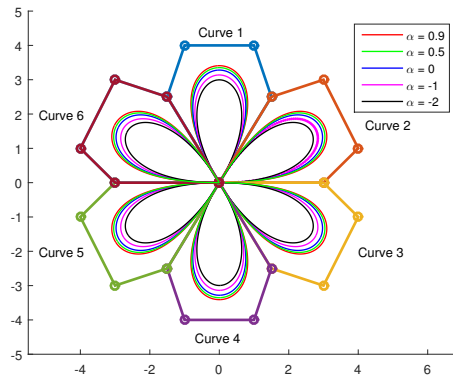
(c) Degree 5

Figure 7: Flower formations using C^0 continuous curves
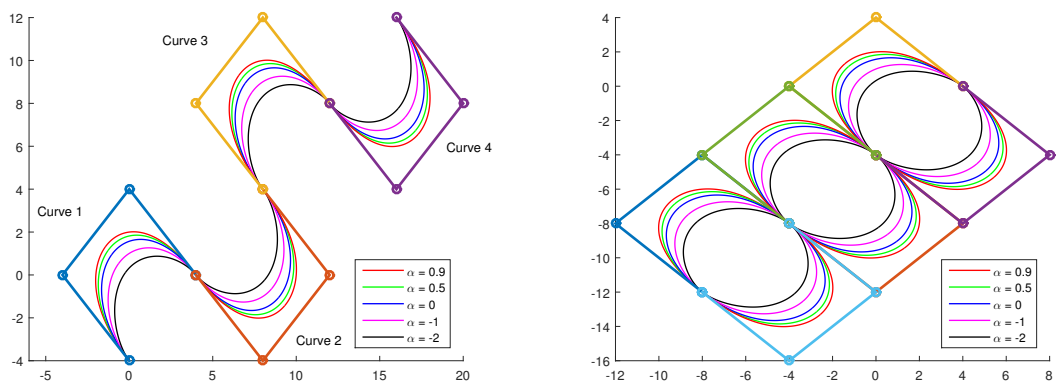
(a) S-shaped pattern

(b) Spiral pattern
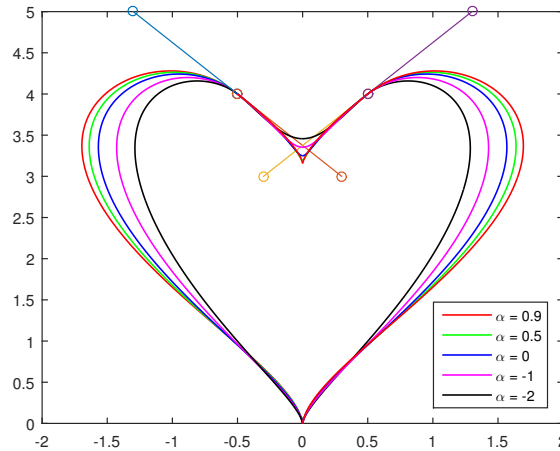
(c) Heart-shaped pattern

Figure 8: Geometric modeling using C^1 continuous curves

are obtained by using equation (12) after substituting α as 0.9. To get the detailed leaf formation, dotted curves in magenta and blue color are extracted by introducing variation in 4th and 5th points obtained after using α as 0.9 in equation (12). Figure 9 (b) discloses the final output drawn using solid and dotted black arcs, in the absence of control polygons.
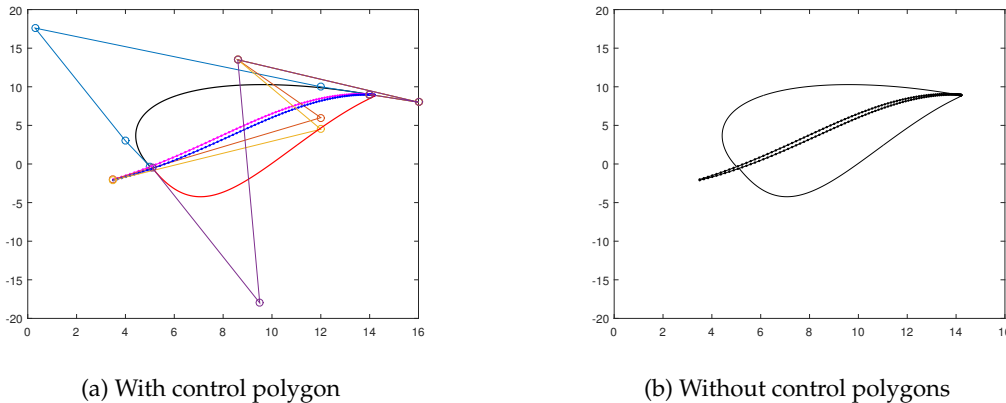
(a) With control polygon

(b) Without control polygons

Figure 9: Leaf formation using C^2 continuous curves

In figure 10 (a), the curve in solid black is formed by substituting α = -1.5 and is joined to the curve in solid red, calculated at α = 0. To draw the tail, multiple curves are calculated that satisfy equation (12), indicated by solid blue for α = 0 and for α = -2, dotted lines in green color are used. The first three control points for the curves represented by dotted lines in green color, are identical. The variation of the last two points is used to form wings in the figure. It is further modeled using black color and detailing is done to demonstrate the overall outcome in figure 10 (b).

The freedom of choosing control points increases as we augment the degree of the curve while dealing with C^3 continuity. This is because first four points of the second curve to be composed are decided according to the continuity constraints and the remaining are chosen independently. In Figure 11 (a)-(b),

(a) Using $\alpha = 1.5$, $\alpha = 0$, $\alpha = -2$

(b) Added details to the graph
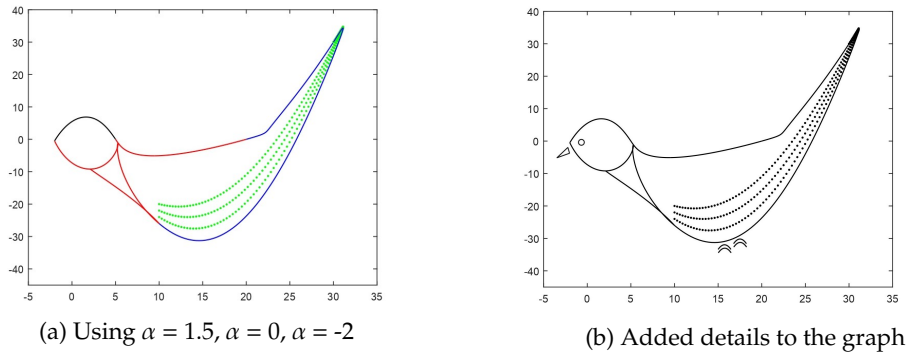
Figure 10: Sparrow formation using C^2 continuous curves

(a) with control polygons

(b) without control polygons
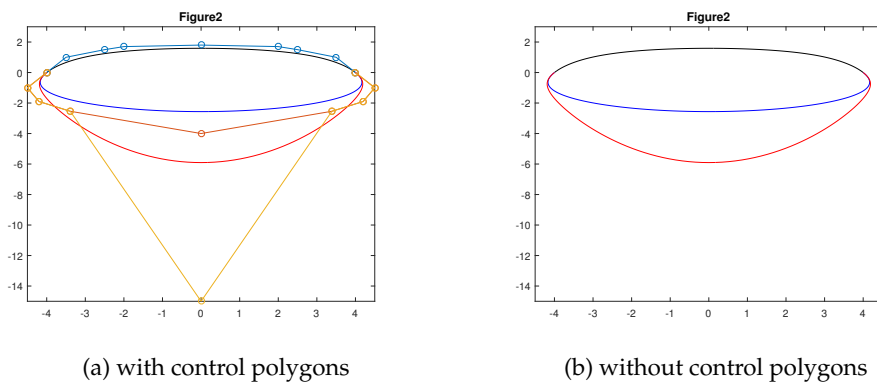
Figure 11: C^3 continuous graphs

curves of degree 8 have been used for which the last five control points are chosen freely, contrary to first four points. Curve traced in black color is composed using (13) for $\alpha = -2$. The third curve drawn in red color is obtained by substituting $\alpha = 0.9$ in (13).

4.2. Geometric continuity constraints of new GBT-Bézier curves

In aviation, the smoothness of materials used in aircraft is a major concern since it impacts the resistance of air and hence affects performance. If we consider computer animation, the transition of the images following a geometric continuous trajectory, results in the depiction of smooth movements per frame. Hence it becomes mandatory to understand the requirements to attain smoothness in these curves.

We introduce the conditions for new GBT-Bézier curves to achieve geometric continuity in this section.
Theorem 4.2: The required and acceptable constraints for geometric continuity of two GBT-Bézier curves defined by using (9) are given below:
1. Conditions for G^0 continuity: G^0 continuity is similar to C^0 continuity. The condition is attained by using:

$$s(\alpha, 0) = q_0 = p_m = r(\alpha, 1). \tag{14}$$

2. Conditions for G^1 continuity: Along with the constraints of G^0 continuity, the curve has to follow additional condition $r(\alpha, 1) = s(\alpha, 0)$ and $r'(\alpha, 1) = \mu \, s'(\alpha, 0)$, provided $\mu > 0$. Thus, we get the constraints for G^1 continuity as:

$$\begin{cases} q_0 = p_m \\ q_1 = \left(\frac{\mu+1}{\mu}\right) p_m - \frac{1}{\mu} p_{m-1}. \end{cases} \tag{15}$$

3. Conditions for G^2 continuity: Along with G^1 continuity constraints, the curves need to have equal curvatures at the point of joining *i.e.* $\kappa_1(1) = \kappa_2(0)$. If $K_1 = r'(\alpha, 1) \times r''(\alpha, 1)$ is the vice normal vector for $r(\alpha, z)$ at $z = 1$ and $K_2 = s'(\alpha, 0) \times s''(\alpha, 0)$ is reverse normal vector for $s(\alpha, z)$ at $z = 0$, then K_1 and K_2 need to have same direction at the joining point to achieve G^2 continuity. Therefore $r'(\alpha, 1)$, $r''(\alpha, 1)$, $s'(\alpha, 0)$ and $s''(\alpha, 0)$ are in the same plane. So, we can write:

$$r''(\alpha, 1) = \zeta\, s''(\alpha, 0) + \tau\, s''(\alpha, 0). \tag{16}$$

Here, $\zeta > 0$ and τ is chosen arbitrarily. On substituting the values of respective curvatures:

$$\begin{aligned}
\kappa_1(1) &= \frac{|r'(\alpha, 1) \times r''(\alpha, 1)|}{|r'(\alpha, 1)|^3} \\
&= \frac{|\mu\, s'(\alpha, 0) \times (\zeta\, s''(\alpha, 0) + \tau\, s'(\alpha, 0))|}{|\mu\, s'(\alpha, 0)|^3} \\
&= \frac{|\mu\, s'(\alpha, 0) \times \zeta\, s''(\alpha, 0)|}{\mu^3\, |s'(\alpha, 0)|^3} \\
&= \frac{\zeta\, |s'(\alpha, 0) \times s''(\alpha, 0)|}{\mu^2\, |s'(\alpha, 0)|^3} \\
&= \kappa_2(0).
\end{aligned} \tag{17}$$

we obtain $\zeta = \mu^2$. Hence the equation (16) is modified to:

$$r''(\alpha, 1) = \mu^2\, s''(\alpha, 0) + \tau\, s'(\alpha, 0). \tag{18}$$

Referring to equation (3), (5) and (6), we substitute the values of $s'(\alpha, 0)$, $s''(\alpha, 0)$ and $r''(\alpha, 1)$ in (18) to get:

$$\begin{aligned}
\beta''_{m-2,m}(\alpha, 1)\, p_{m-2} \;+\; \beta''_{m-1,m}(\alpha, 1)\, p_{m-1} \;+\; \beta''_{m,m}(\alpha, 1)\, p_m &= \mu^2 \left[\beta''_{0,m}(\alpha, 0)\, q_0 + \beta''_{1,m}(\alpha, 0)\, q_1 + \beta''_{2,m}(\alpha, 0)\, q_2 \right] \\
&\quad + \tau \left[\beta'_{0,m}(\alpha, 0)\, q_0 + \beta'_{1,m}(\alpha, 0)\, q_1 \right].
\end{aligned} \tag{19}$$

By comparing the values between $\beta''_{0,m}(\alpha, 0)$ and $\beta''_{0,m}(\alpha, 1)$ in (5) & (6) and using G^1 continuity conditions in (15), we re-write (19) as:

$$\begin{aligned}
\beta''_{2,m}(\alpha, 0)p_{m-2} + \beta''_{1,m}(\alpha, 0)p_{m-1} + \beta''_{0,m}(\alpha, 0)p_m &= \mu^2 \left[\beta''_{0,m}(\alpha, 0)p_m + \beta''_{1,m}(\alpha, 0)\left(\left(\frac{\mu + 1}{\mu}\right)p_m - \frac{1}{\mu}p_{m-1} \right) + \beta''_{2,m}(\alpha, 0)q_2 \right] \\
&\quad + \tau \left[\beta'_{0,m}(\alpha, 0)p_m + \beta'_{1,m}(\alpha, 0)\left(\left(\frac{\mu + 1}{\mu}\right)p_m - \frac{1}{\mu}p_{m-1} \right) \right].
\end{aligned} \tag{20}$$

On simplifying the above equation, we obtain:

$$\begin{aligned}
q_2 &= \frac{1}{\mu^2}p_{m-2} - \left(\frac{\mu + 1}{\mu^2}\right)\left[\frac{\beta''_{1,m}(\alpha, 0)}{\beta''_{2,m}(\alpha, 0)}\right][\mu p_m - p_{m-1}] - \frac{\tau}{\mu^3}\left[\frac{\beta'_{1,m}(\alpha, 0)}{\beta''_{2,m}(\alpha, 0)}\right][(\mu + 1)p_m - p_{m-1}] \\
&\quad + \frac{1}{\mu^2}\left[\frac{\beta''_{0,m}(\alpha, 0)(1 - \mu^2) - \beta'_{0,m}(\alpha, 0)\tau}{\beta''_{2,m}(\alpha, 0)}\right]p_m.
\end{aligned} \tag{21}$$

By using the endpoint properties of the curves, we get the following constraints for G^2 continuity:

$$\begin{cases} q_0 = p_m \\ q_1 = \left(\frac{\mu+1}{\mu}\right)p_m - \frac{1}{\mu}p_{m-1} \\ \\ q_2 = \frac{1}{\mu^2}p_{m-2} - \left(\frac{\mu+1}{\mu^2}\right)\left[\frac{\beta''_{1,m}(\alpha,0)}{\beta''_{2,m}(\alpha,0)}\right](\mu p_m - p_{m-1}) \\ \\ \qquad - \frac{\tau}{\mu^3}\left[\frac{\beta'_{1,m}(\alpha,0)}{\beta''_{2,m}(\alpha,0)}\right][(\mu+1)p_m - p_{m-1}] \\ \\ \qquad + \frac{1}{\mu^2}\left[\frac{\beta''_{0,m}(\alpha,0)(1-\mu^2)-\beta'_{0,m}(\alpha,0).\tau}{\beta''_{2,m}(\alpha,0)}\right]p_m. \end{cases} \tag{22}$$

On substituting $\mu = 1$ and $\tau = 0$, we get (10). Hence, G^2 continuity constraints are reducible to C^2 continuity constraints.

4. Conditions for G^3 continuity: As we proceed to calculate G^3 continuity conditions, it is to be noted that the derivative of curvature of the curves needs to be equal at the point of junction (*i.e.* $\kappa'_1(1) = \mu\kappa'_2(0)$) in addition to G^2 continuity constraints. Therefore we have the derivative of curvatures of the two curves at endpoints as:

$$\begin{cases} \kappa'_1(1) = \dfrac{\|r'(.,1)\|^2 \{r'(.,1) \times r'''(.,1)\} - 3\{r'(.,1) \times r''(.,1)\}\{r'(.,1).r''(.,1)\}}{\|r'(.,1)\|^5} \\ \\ \kappa'_2(0) = \dfrac{\|s'(.,0)\|^2 \{s'(.,0) \times s'''(.,0)\} - 3\{s'(.,0) \times s''(.,0)\}\{s'(.,0).s''(.,0)\}}{\|s'(.,0)\|^5}. \end{cases} \tag{23}$$

So in order to be G^3 continuous, the curves need to satisfy the following conditions:

$$\begin{cases} r(\alpha,1) = s(\alpha,0) \\ r'(\alpha,1) = \mu s'(\alpha,0) \\ r''(\alpha,1) = \mu^2 s''(\alpha,0) + \tau s'(\alpha,0) \\ r'''(\alpha,1) = \xi s'''(\alpha,0) + 3\mu\tau s''(\alpha,0) + \tau s'(\alpha,0). \end{cases} \tag{24}$$

Considering $\kappa'_1(1)$ and by using equation (24) we get

$$\begin{aligned} \kappa'_1(1) &= \frac{\|r'(.,1)\|^2 \{r'(.,1) \times r'''(.,1)\} - 3\{r'(.,1) \times r''(.,1)\}\{r'(.,1).r''(.,1)\}}{\|r'(.,1)\|^5} \\ \\ &= \frac{\|\mu s'(.,0)\|^2 \left\{\mu s'(.,0) \times (\xi s'''(.,0) + 3\mu\tau s''(.,0) + \tau s'(.,0))\right\}}{\|\mu s'(.,0)\|^5} \\ \\ &\quad - \frac{3\left\{\mu s'(.,0) \times (\mu^2 s''(.,0) + \tau s'(.,0))\right\}\left\{\mu s'(.,0).(\mu^2 s''(.,0) + \tau s'(.,0))\right\}}{\|\mu s'(.,0)\|^5} \\ \\ &= \mu\kappa'_2(0). \end{aligned} \tag{25}$$

We get $\xi = \mu^3$ and hence

$$r'''(\alpha,1) = \mu^3 s'''(\alpha,0) + 3\mu\tau s''(\alpha,0) + \tau s'(\alpha,0). \tag{26}$$

Referring to equation (3),(5), (7) and (8), we substitute the values of $s'(\alpha, 0)$, $s''(\alpha, 0)$, $s'''(\alpha, 0)$ and $r'''(\alpha, 1)$ in (19) to get:

$$
\begin{aligned}
\beta'''_{m-3,m} p_{m-3}(\alpha, 1) + \beta''_{m-2,m}(\alpha, 1) p_{m-2} + \beta''_{m-1,m}(\alpha, 1) p_{m-1} + \beta''_{m,m}(\alpha, 1) p_m &= \mu^3 \Big[\beta'''_{0,m}(\alpha, 0) q_0 + \beta'''_{1,m}(\alpha, 0) q_1 \\
&\quad + \beta'''_{2,m}(\alpha, 0) q_2 + \beta'''_{3,m}(\alpha, 0) q_3 \Big] \\
&\quad + 3\mu\tau \Big[\beta''_{0,m}(\alpha, 0) q_0 + \beta''_{1,m}(\alpha, 0) q_1 \\
&\quad + \beta''_{2,m}(\alpha, 0) q_2 \Big] + \tau \Big[\beta'_{0,m}(\alpha, 0) q_0 + \beta'_{1,m}(\alpha, 0) q_1 \Big].
\end{aligned}
\tag{27}
$$

On simplifying the above equation, we obtain:

$$
\begin{aligned}
q_3 &= -\frac{p_{m-3}}{\mu^3} - \left[\left(\frac{1}{\mu^3} + \frac{1}{\mu^2} \right) p_{m-2} - \left(\frac{\mu+1}{\mu^2} \right) \frac{\beta''_{1,m}(\alpha, 0)}{\beta''_{2,m}(\alpha, 0)} (\mu p_m - p_{m-1}) - \frac{\tau}{\mu^3} \frac{\beta'_{1,m}(\alpha, 0)}{\beta''_{2,m}(\alpha, 0)} \Big[(\mu + 1) p_m - p_{m-1} \Big] \right] \frac{\beta'''_{2,m}(\alpha, 0)}{\beta'''_{3,m}(\alpha, 0)} \\
&\quad - \frac{p_m}{\mu^2} \left[\frac{\beta''_{0,m}(\alpha, 0)(1 - \mu^2) - \beta'_{0,m}(\alpha, 0)\tau}{\beta''_{2,m}(\alpha, 0)} \right] \frac{\beta'''_{2,m}(\alpha, 0)}{\beta'''_{3,m}(\alpha, 0)} - \frac{3\tau}{\mu^2} \Big[\beta''_{0,m}(0) q_0 + \beta''_{1,m}(0) q_1 + \beta''_{2,m}(0) q_2 \Big] \frac{1}{\beta'''_{3,m}(\alpha, 0)} \\
&\quad - \frac{\tau}{\mu^3} \Big[\beta'_{0,m}(0) q_0 + \beta'_{1,m}(0) q_1 \Big] \frac{1}{\beta'''_{3,m}(\alpha, 0)}.
\end{aligned}
\tag{28}
$$

By using the endpoint properties of the curves, we get the following constraints for G^3 continuity:

$$
\begin{cases}
q_0 = p_m \\
q_1 = \left(\frac{\mu+1}{\mu} \right) p_m - \frac{1}{\mu} p_{m-1} \\[2mm]
q_2 = \frac{1}{\mu^2} p_{m-2} - \left(\frac{\mu+1}{\mu^2} \right) \left[\frac{\beta''_{1,m}(\alpha,0)}{\beta''_{2,m}(\alpha,0)} \right] (\mu p_m - p_{m-1}) \\[2mm]
\qquad - \frac{\tau}{\mu^3} \left[\frac{\beta'_{1,m}(\alpha,0)}{\beta''_{2,m}(\alpha,0)} \right] \Big[(\mu + 1) p_m - p_{m-1} \Big] \\[2mm]
\qquad + \frac{1}{\mu^2} \left[\frac{\beta''_{0,m}(\alpha,0)(1 - \mu^2) - \beta'_{0,m}(\alpha,0).\tau}{\beta''_{2,m}(\alpha,0)} \right] p_m \\[3mm]
q_3 = -\frac{p_{m-3}}{\mu^3} - \left[\left(\frac{1}{\mu^3} + \frac{1}{\mu^2} \right) p_{m-2} - \left(\frac{\mu+1}{\mu^2} \right) \frac{\beta''_{1,m}(\alpha,0)}{\beta''_{2,m}(\alpha,0)} (\mu p_m - p_{m-1}) - \frac{\tau}{\mu^3} \frac{\beta'_{1,m}(\alpha,0)}{\beta''_{2,m}(\alpha,0)} \Big[(\mu + 1) p_m - p_{m-1} \Big] \right] \frac{\beta'''_{2,m}(\alpha,0)}{\beta'''_{3,m}(\alpha,0)} \\[2mm]
\qquad - \frac{p_m}{\mu^2} \left[\frac{\beta''_{0,m}(\alpha,0)(1 - \mu^2) - \beta'_{0,m}(\alpha,0)\tau}{\beta''_{2,m}(\alpha,0)} \right] \frac{\beta'''_{2,m}(\alpha,0)}{\beta'''_{3,m}(\alpha,0)} - \frac{3\tau}{\mu^2} \Big[\beta''_{0,m}(\alpha, 0) q_0 + \beta''_{1,m}(\alpha, 0) q_1 + \beta''_{2,m}(\alpha, 0) q_2 \Big] \frac{1}{\beta'''_{3,m}(\alpha,0)} \\[2mm]
\qquad - \frac{\tau}{\mu^3} \Big[\beta'_{0,m}(\alpha, 0) q_0 + \beta'_{1,m}(\alpha, 0) q_1 \Big] \frac{1}{\beta'''_{3,m}(\alpha,0)}.
\end{cases}
\tag{29}
$$

On substituting $\mu = 1$ and $\tau = 0$, we get (13). Hence, G^3 continuity constraints are reducible to C^3 continuity constraints.

4.2.1. Applications based on geometric continuity

The augmentation of classical Bézier curves is done with the help of newly defined GBT-Bézier curves which are extensively used to understand the mathematics involved in CAD/CAGD. Moreover, geometric continuities of these curves provide leverage in computer animation, curve tracing, and alphabet formations as discussed in figure 12- 15. While working with complex shapes that follow geometric continuity, multiple curves are composed together. Figure 12 lays out the composition of G^0 continuous curves for the same.
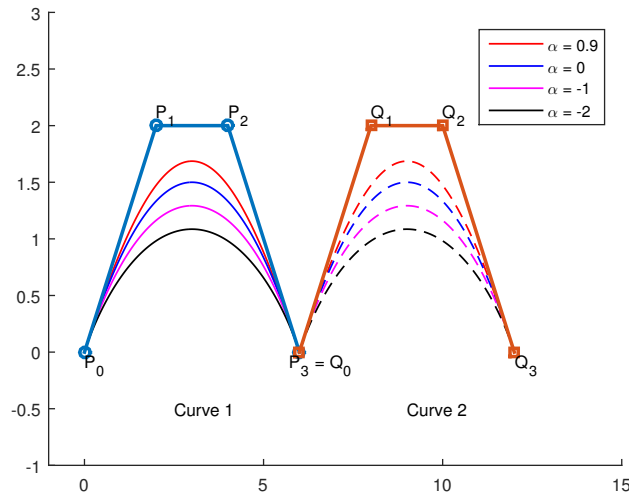
Figure 12: Composition of G^0 continuous curves

Figure 13 (a) demonstrates the modeling of cubic G^1 continuous curves. The curves in black color are outlined at $\alpha = 0.9$. Blue color manifests G^1 continuous curves calculated using equation (15) for $\alpha = -1$, $\mu = 0.8$ and curves in red satisfy G^1 continuity for $\alpha = -1$ and $\mu = 2$. A ball and line segments at the grip of the hockey sticks are drawn to add details to the figure. Likewise in Figure 13 (b), cursive alphabet "B" (initial letter for "Bézier") is sketched. Initial curve is formed at $\alpha = 0.9$ in black color, which is composed of a curve drawn in red color after substituting $\alpha = -1.5$ and $\mu = 2$ in equation (15). Curves in magenta and blue are traced for the control points fetched after satisfying equation (15) at $\alpha = -1.5$ and $\mu = 2$. A little swirl using black color is added at the end of the last curve to complete the formation.

(a) Hockey formation

(b) Alphabet formation
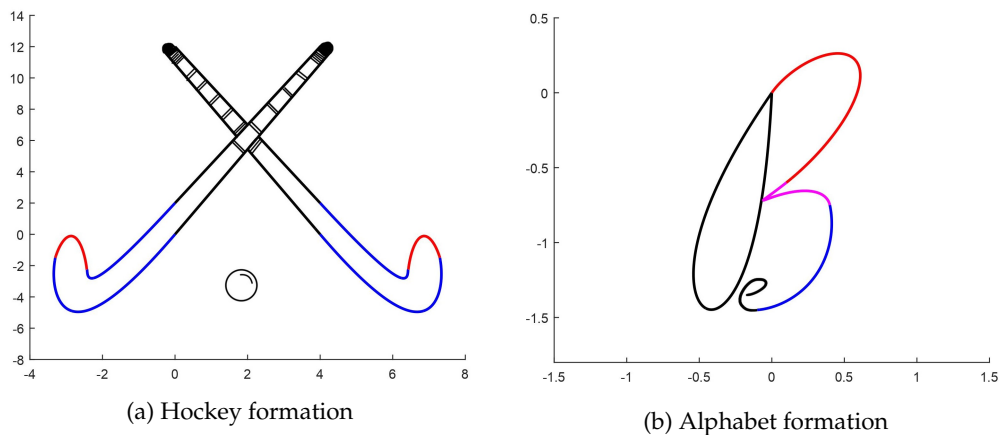
Figure 13: G^1 continuous curves

Figure 14 (a) consists of cat formation for which α is taken as 0.9 to draw the curves represented using black color. Red arcs are formed at $\alpha = 0.9$. The G^2 continuity is achieved as the curves in red color, conjunct the curve in blue for $\alpha = 0.95$, $\mu = 2$, and $\tau = -3$. The tail of the cat is drawn to polish the final figure. In figure 14 (b), the given shuttle shows G^2 continuity at the cork as the two curves in red and blue associate with each other. The initial curve is formed at $\alpha = 0.9$. Conditions of G^2 continuity are satisfied by the curves in red color for $\alpha = 0.86$, $\mu = 4$ and $\tau = 2$. Similar values are used to get the control points for the curve traced in blue color. Horizontal lines are drawn to beautify the image.

(a) Cat formation   (b) Shuttle formation
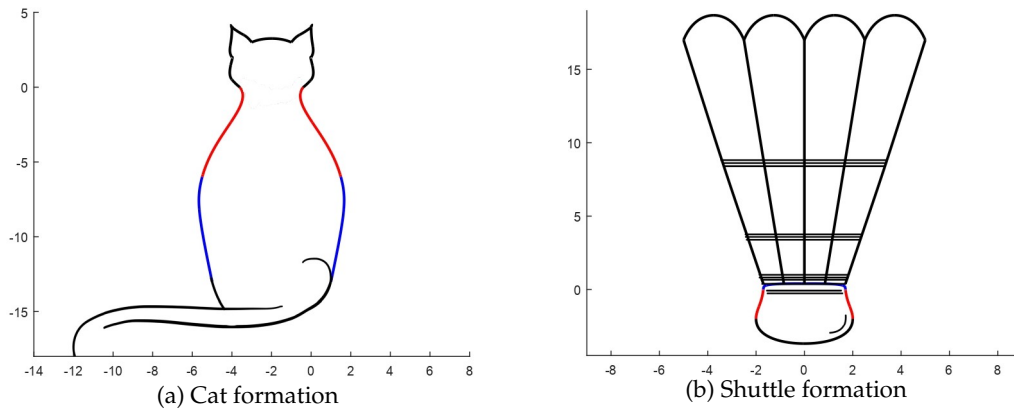
Figure 14: G^2 continuous curves

(a) With control polygon   (b) Without control polygons
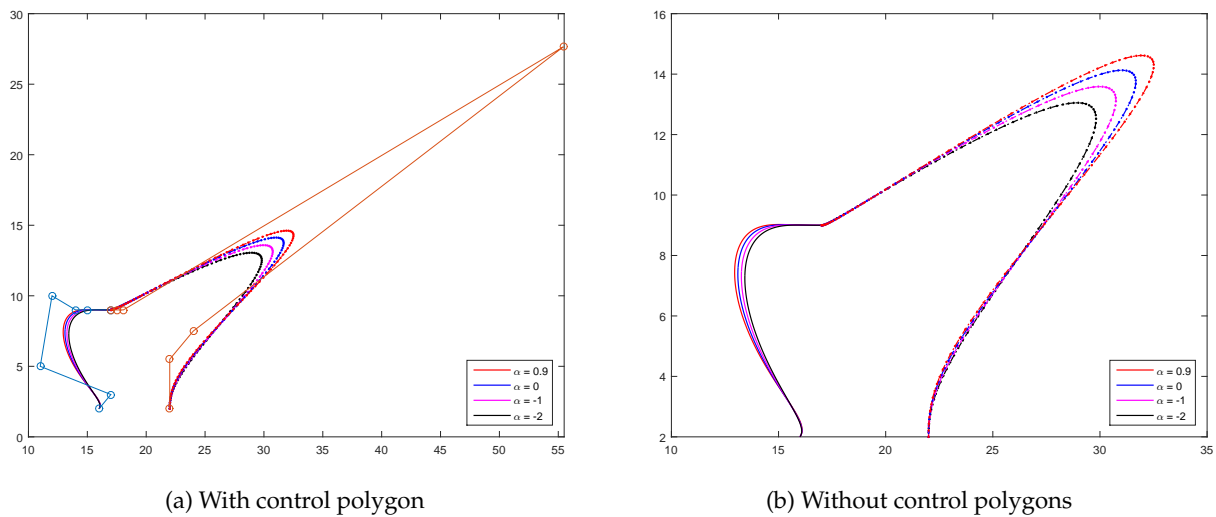
Figure 15: G^3 continuous curves

Figure 15 (a) demonstrates the composition of two curves of degree 6 that are G^3 continuous. For $\tau = 2$ and $\mu = 4$, varying values of α are considered. Solid lines indicate the variation in the first curve for α taken as 0.9, 0, -1, and -2 for which red, blue, magenta, and black colors are used respectively. The dotted lines indicate the second curve under consideration which is obtained after applying G^3 continuity conditions. Figure 15 (b) represents an enlarged version (without control polygon) of G^3 continuous curves taken in Figure 15 (a).

Figure 16 compares classical Bézier, T-Bézier [11], GT-Bézier [18], GBT-Bézier [19] and new GBT-Bézier curves represented by green, red, black, blue and magenta color respectively. For positive values of various shape parameters as given in 16 (a), it is observed that new GBT-Bézier curves approximate better than classical and GT-Bézier curves till the midpoint of segment BC. Beyond that, it appears to be more suitable for structures that require smoother bends. Parallel to that, figure 16 (b) demonstrates that for the negative values of shape parameters, new GBT-Bézier curve approximates better than the GT-Bézier, GBT-Bézier and T-Bézier curves once the midpoint of the segment BC is crossed. Though T-Bézier curves appear to be the closest to control polygon as we trace the segment AB in 16 (a), these are not C^1 continuous curves for all
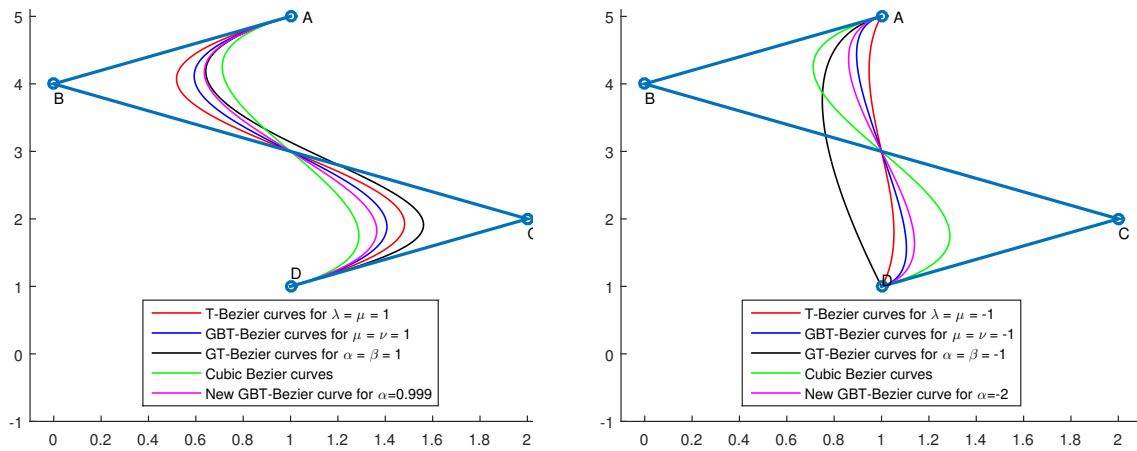
(a) For positive values of parameters

(b) For negative values of parameters

Figure 16: Comparing cubic Bézier curves formed by using different basis functions

$\lambda, \mu \in [-2, 1]$. Hence these can't be used for the curve modeling that demands parametric continuities higher than C^0 for all $\lambda, \mu \in [-2, 1]$. It has to be noted that for different requirements of curve tracing, different basis functions serve the purpose accordingly. Bases that use more than one parameter, are symmetrical only when all the parameters have identical values. On the other hand, if we use a single parameter, it reduces the computational cost that links to the curves generated by such bases and the resultant basis functions are symmetrical throughout. Hence new GBT-Bézier curves provide an advantage in this context as well. For further comparison between the earlier available basis functions [15] can be referred.

5. Conclusion

New generalized blended trigonometric Bézier-like functions have been formulated in this paper. Basic properties of classical Bézier curves are satisfied by the new GBT-Bézier curves with additional flexibility to alter the shape of the curves without changing the control polygon. With the increasing value of parameter α, the curves are traced closer to the control polygon.
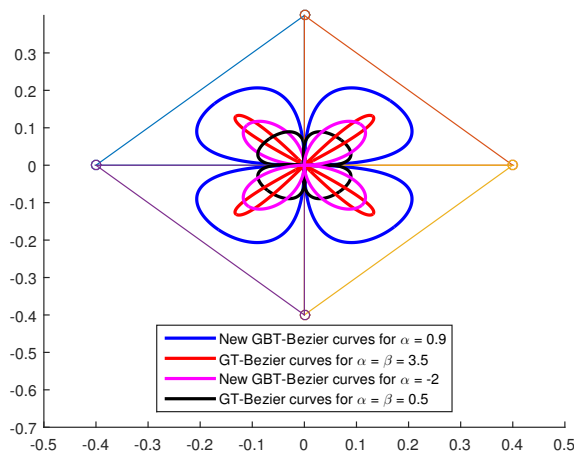
Figure 17: Comparison between new GBT and GT Bézier curves

It is evident from Figure 17 that the new GBT-Bernstein basis approximates the curves better for $\alpha = 0.9$ as compared to the basis formulated by [3] for $\alpha = \beta = 3.5$.

The conditions for parametric and geometric continuity have been constructed for the composition of newly generated GBT-Bézier curves. Multi-fold formations presented as applications to the proposed basis reveal that the new basis functions can be used for CAG/CAD modeling.

6. Declaration of Competing Interest

The authors affirm that they have no known financial or personal affiliations that would have appeared to conflict with the work described in this study.

7. Acknowledgment

References

[1] T. Acar, P. N. Agrawal, T. Neer, *Bézier variant of the Bernstein–Durrmeyer type operators*, Results Math. **72** (2017), 1341–1358.
[2] T. Acar, A. Kajla, *Blending type approximation by Bézier-summation-integral type operators*, Commun. Fac. Sci. Univ. Ank. Ser. A1. Math. Stat. **67(2)** (2018), 195–208.
[3] M. Ammad, M. Y. Misro, A. Ramli, *A novel generalized trigonometric Bézier curve: properties, continuity conditions and applications to the curve modeling*, Math. Comput. Simulation **194** (2022), 744–763.
[4] U. Bashir, M. Abbas, M. N. H. Awang, J. M. Ali, *A class of quasi-quintic trigonometric Bézier curve with two shape parameters*, Sci. Asia **39(2)** (2013), 11–15.
[5] S. BiBi, M. Abbas, M. Y. Misro, G. Hu, *A novel approach of hybrid trigonometric Bézier curve to the modeling of symmetric revolutionary curves and symmetric rotation surfaces*, IEEE Access **7(1)** (2019), 165779–165792.
[6] S. BiBi, M. Abbas, K. T. Miura, M. Y. Misro, *Geometric modeling of novel generalized hybrid trigonometric Bézier-like curve with shape parameters and its applications*, Mathematics **8(6)** (2020), 967–996.
[7] M. Dube, R. Sharma, *Quartic trigonometric Bézier curve with a shape parameter*, Int. J. Math. Comput. Appl. Res. **3(3)** (2013), 89–96.
[8] X. Han, *Quadratic trigonometric polynomial curves with a shape parameter*, Comput. Aided Geom. Design **19(7)** (2002), 503–512.
[9] X. A. Han, X. Huang, Y. Ma, *Shape analysis of cubic trigonometric Bézier curves with a shape parameter*, Appl. Math. Comput. **217(6)** (2010), 2527–2533.
[10] X. A. Han, Y. Ma, X. Huang, *A novel generalization of Bézier curve and surface*, J. Comput. Appl. Math. **217(1)** (2008), 180–193.
[11] X. A. Han, Y. Ma, X. Huang, *The cubic trigonometric Bézier curve with two shape parameters*, Appl. Math. Lett. **22(2)** (2009), 226–231.
[12] G. Hu, C. Bo, X. Qin, *Continuity conditions for Q-Bézier curves of degree n*, J. Inequal. Appl. **2017(1)** (2017), 1–14.
[13] A. Kajla, *On the Bézier variant of the Srivastava-Gupta operators*, Constr. Math. Anal. **1(2)** (2018), 99–107.
[14] A. Kajla, T. Acar, *Bézier–Bernstein–Durrmeyer type operators*, Rev. R. Acad. Cienc. Exactas Fís. Nat. Ser. A Math. RACSAM **114** (2020), 1–11.
[15] H. Kaur, M. R. Goyal, *A comparative analysis of different basis functions for constructing Bézier curves*, In the proceedings of ICMMAAC 2022, Lect. Notes Netw. Syst. **666** (2022), 413–423.
[16] J. Li, D. Zhao, *An investigation on image compression using the trigonometric Bézier curve with a shape parameter*, Math. Probl. Eng. **2013** (2013), 1–8.
[17] A. Majeed, M. Abbas, A. A. Sittar, M. Kamran, S. Tahseen, H. Emadifar, *New cubic trigonometric Bézier-like functions with shape parameter: Curvature and its spiral segment*, J. Math. **2021** (2021), 1–13.
[18] S. Maqsood, M. Abbas, G. Hu, A. L. A. Ramli, K. T. Miura, *A novel generalization of trigonometric Bézier curve and surface with shape parameters and its applications*, Math. Probl. Eng. **2020** (2020), 1–25.
[19] S. Maqsood, M. Abbas, K. T. Miura, A. Majeed, A. Iqbal, *Geometric modeling and applications of generalized blended trigonometric Bézier curves with shape parameters*, Adv. Differ. Equ. 2020 (2020), 1–18.
[20] M. Y. Misro, A. Ramli, J. M. Ali, *Quintic trigonometric Bézier curve with two shape parameters*, Sains Malays. **46** (2017), 825–831.
[21] S. Naseer, M. Abbas, H. Emadifar, S. BiBi, T. Nazir, Z. H. Shah, *A class of sextic trigonometric Bézier curve with two shape parameters*, J. Math. **2021** (2021), 1–16.
[22] D. Occorsio, M. G. Russo, W. Themistoclakts, *Some numerical applications of generalized Bernstein operators*, Constr. Math. Anal. **4(2)** (2021), 186–214.

[23] D. Páleš, J. Rédl, Bézier curve and its application, Math. Educ. Res. Appl. **1(2)** (2015), 49–55.
[24] R. Sharma, *Quartic trigonometric Bézier curves and surfaces with shape parameters*, Int. J. Innov. Res. Comput. Commun. Eng. **4(4)** (2016), 7712–7717.
[25] R. Sharma, *Cubic trigonometric Bézier curve with shape parameter*, Int. J. Innov. Res. Comput. Commun. Eng. **4(4)** (2016), 7718–7723.
[26] M. Usman, M. Abbas, K. T. Miura, *Some engineering applications of new trigonometric cubic Bézier-like curves to free-form complex curve modeling*, J. Adv. Mech. Des. Syst. Manuf. **14(4)** (2020), 1–15.
[27] B. Uzma, M. Abbas, M. N. H. Awang, J. M. Ali, *The quadratic trigonometric Bézier curve with single shape parameter*, J. Basic Appl. Sci. Res. **2(3)** (2012), 2541–2546.